AIP | Applied Physics Letters

Fano resonance based optical modulator reaching 85% modulation depth

Wenyu Zhao, Huan Jiang, Bingyi Liu, Yongyuan Jiang, Chengchun Tang, and Junjie Li

Citation: Applied Physics Letters **107**, 171109 (2015); doi: 10.1063/1.4935031
View online: http://dx.doi.org/10.1063/1.4935031
View Table of Contents: http://scitation.aip.org/content/aip/journal/apl/107/17?ver=pdfcov
Published by the AIP Publishing

Fano resonance based optical modulator reaching 85% modulation depth

Wenyu Zhao,[1] Huan Jiang,[1] Bingyi Liu,[1] Yongyuan Jiang,[1,2,a)] Chengchun Tang,[3] and Junjie Li[3]
[1]*Department of Physics, Harbin Institute of Technology, Harbin 150001, China*
[2]*Key Laboratory of Micro-Optics and Photonic Technology of Heilongjiang Province, Harbin 150001, China*
[3]*Beijing National Laboratory for Condensed Matter Physics, Institute of Physics, Chinese Academy of Sciences, P.O. Box 603, Beijing 100190, China*

(Received 7 September 2015; accepted 21 October 2015; published online 29 October 2015)

In this paper, we demonstrate the combination of nematic liquid crystal with a binary silicon nanohole array to realize a high performance Fano resonance based optical modulator. The simulations using a finite difference time domain method reveal that the sharp Fano profile in the binary array originates from the interaction of the in-phased and anti-phased lattice collective resonance hybridized through lattice coupling effects. Experimental results agree very well with the simulations and demonstrate the strong dependence of the Q factor and spectral contrast of the resonance on the radius difference of the two nanohole arrays. Infiltrated with nematic liquid crystal, E7, the Fano profile can be dynamically and continuously tuned by an applied voltage, and an unprecedented modulation depth up to 85% is achieved. © *2015 AIP Publishing LLC*. [http://dx.doi.org/10.1063/1.4935031]

Active plasmonics enabling real-time control over nano-devices' properties have attracted a tremendous amount of attention in the past few years.[1–4] Great progress has been made towards a wealth of promising applications such as active catalysis,[5] optical nanoantennas,[6] solar cells,[7] and biological sensing and imaging.[8] Among the various active tuning media, such as stimuli-responsive polymers,[9] photochromic molecules[10] and inorganic phase-transition materials,[11] liquid crystal (LC) is an excellent candidate because of its relatively large birefringence on refractive index and versatile driven methods to stimulate molecule realignment.[1,2] Many research works have been conducted to incorporate the LC into metal nanostructures to manipulate the transmission or the reflection of the plasmonic structures, which have potentials for color filters, nano-switches, and nano-modulators.[12–19] However, due to the low Q factor and poor spectral contrast of the resonances in metal nanostructures, the modulation depths underpinning most nano-devices are limited to rather small values posing a great obstacle for practical applications. Improving the performance of modulation depth remains a major challenge and more research efforts are desirable.

Recently, Fano resonances in nanostructures resulting from the interaction of "dark states" and "bright states" have been extensively studied.[20,21] Due to the high Q factor and spectral contrast, Fano resonances have been employed in many applications where sharp resonances are essential for the performances such as biosensors,[22] filters,[23] surface-enhanced Raman scattering (SERS),[24] and surface plasmon lasers.[25] More recently, we demonstrated a binary silicon particle array and studied the multi-trapped modes and corresponding Fano resonances resulting from the lattice coupling effects in the array.[26] Because of the low loss nature of dielectric,[27–29] the Q factor and spectral contrast of such Fano resonances can be strongly improved simultaneously resulting in an ultra-high figure of merit that is orders higher than its conventional counterparts made of metal.

In this paper, we take advantage of the easy tuning mechanism of nematic LC and the high Q factor and spectral contrast of the Fano resonance in a binary nanohole array perforated in a silicon film to realize a high performance optical modulator. Simulations using finite difference time domain method demonstrate that the origin of the sharp asymmetric profile supported by the binary nanohole array is related to the excitations of the anti-phased lattice collective resonance (ALCR) and the in-phased lattice collective resonance (ILCR) hybridized through lattice coupling effects. Experimental results and simulations are in very good agreement and show the strong dependence of the Q factor and spectral contrast on the radius difference between the two nanohole arrays. We then incorporate commercial E7 LC into the binary nanohole array and study the performance of such structure as optical modulator. The Fano profile dynamically shifts towards the short wavelength as the applied voltage gradually increases from 0 to 26.7 kV/cm, and modulation depth up to 85% can be realized for the operating wavelength of 713 nm.

Fig. 1(a) shows the artistic impression of the binary nanohole array composed of two nanohole arrays with different radii of R_1 and R_2 perforated in a silicon film ($H = 30$ nm). The periods of the two arrays are both P (400 nm) and the centers of the nanoholes have a displacement of half period. In order to fabricate the binary nanohole array, a layer of amorphous silicon film is deposited using plasma enhanced chemical vapor deposition (PECVD) method on a glass substrate pre-deposited an indium tin oxide (ITO) layer of 20 nm as electrode. The binary nanohole arrays with footprints of 100 μm × 100 μm are then fabricated using standard electron beam lithography followed by ion beam etching process (Fig. 1(c)). To measure the transmission of the samples, white light from a halogen tungsten lamp is focused on a spot size of nearly 50 μm in diameter by a 5× objective, and then on the other side collected by another 20× objective and transmitted to an optical fiber spectrometer (USB2000+, Ocean

a)Author to whom correspondence should be addressed. Electronic mail: jiangyy@hit.edu.cn

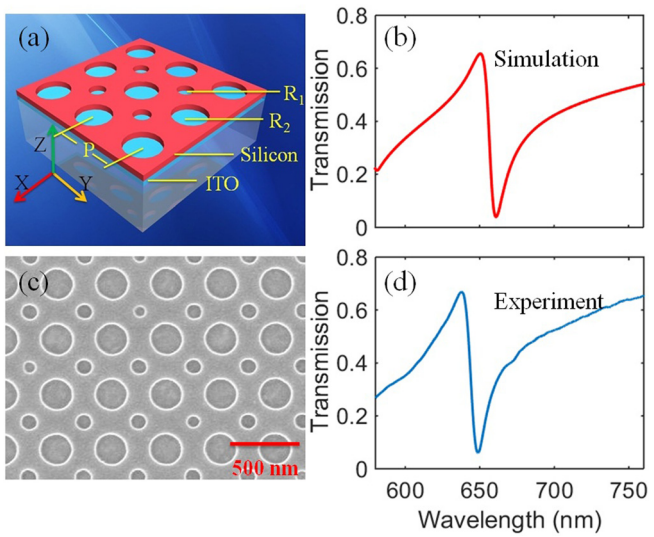

FIG. 1. (a) Artistic impression of binary silicon nanohole array with different radii of R_1 and R_2. (b) Calculated transmission using FDTD Solutions. (c) Scanning electron microscope (SEM) image and (d) measured transmission of the fabricated binary nanohole array for $R_1 = 50$ nm and $R_2 = 110$ nm.

Optics). The simulations are conducted using commercial finite difference time domain method software, FDTD Solutions from Lumerical, Inc. The permittivity of glass, silicon, and ITO are extracted from the experimental data.[30,31]

A sharp Fano resonance with a high spectral contrast (Fig. 1(b)) appears in transmission around 650 nm, and the Fano profile evolves from a dip of 4% transmission to a peak of 65% transmission within 10 nm. Measured transmission (Fig. 1(d)) agrees very well with the simulation results except a slight deviation of resonance wavelength mainly due to the deviations of geometric parameters caused during fabrication process. The distinct Fano profile can be explained using the hybridization theory;[26] each nanohole array supports corresponding lattice collective resonance which is the lattice collective excitations of the cavity modes supported by the constituent nanoholes in the array.[32] When two nanohole arrays with different radii are combined to form a binary one, the two supported lattice collective resonance modes with different resonant energies will hybridize to generate the ILCR mode and ALCR mode through lattice coupling effects. In the ILCR mode, two nanohole arrays will always oscillate towards the same direction either in-phase or anti-phase with the incident light; thus, the reradiated fields of the two nanohole arrays interfere constructively in the far field resulting in an enhanced radiation to the free space. The ILCR mode is termed as "bright mode" because of its enhanced scattering and effective coupling to the incident light. In the ALCR mode, two arrays will oscillate towards the opposite directions, leading to the destructive reradiated fields in the far field and strong elimination of scattering loss. This resonant mode can be considered the "dark mode" due to its long lifetime and weak coupling to the free space radiation. The interaction of the ALCR mode and ILCR mode gives rise to the sharp asymmetric Fano profile in transmission.

To interpret the ALCR mode and ILCR mode more clearly, we plot the phase map of the electric field of the binary array for a unit cell at the plane across the centers of each nanohole ($Z = 15$ nm). Figs. 2(a) and 2(b) correspond to the phase map at 660 nm and 740 nm ($R_1 = 50$ nm and $R_2 = 110$ nm), respectively. The excited cavity modes in the

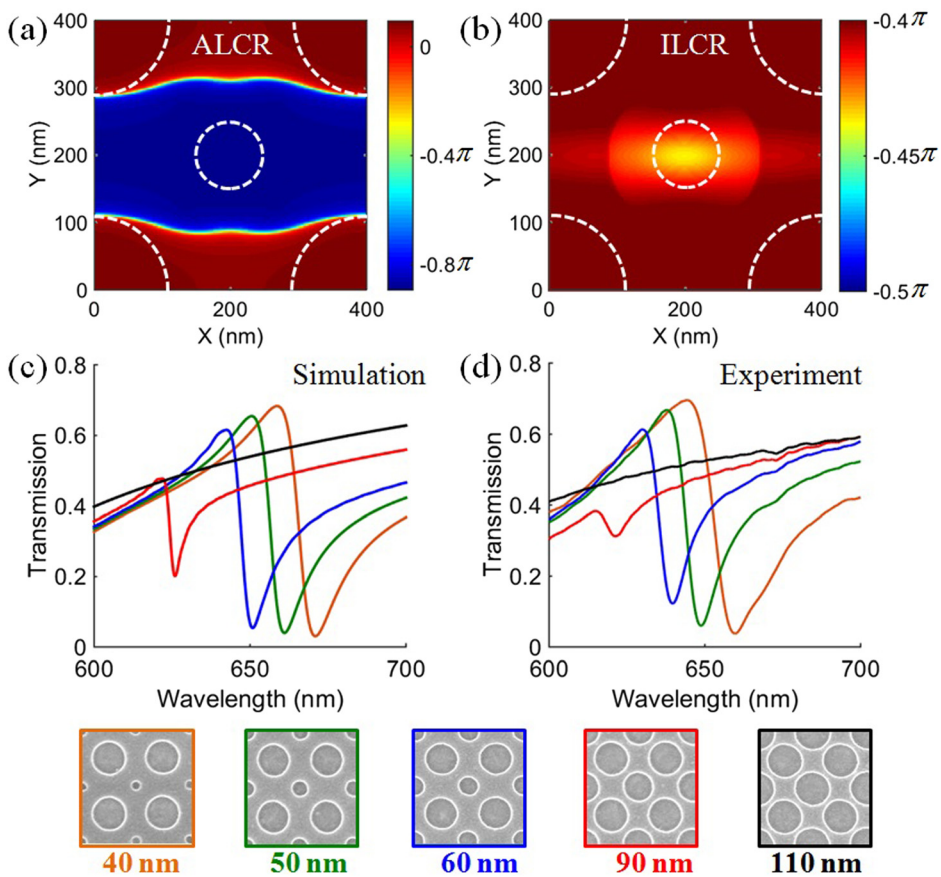

FIG. 2. Phase maps of the electric field of the binary nanohole array for a unit cell at the plane across the centers of each nanohole ($Z = 15$ nm) for (a) ALCR mode and (b) ILCR mode. Transmission of the binary nanohole array for different R_1, while R_2 is fixed at 110 nm extracted from (c) simulations and (d) experiments. The bottom row shows the corresponding SEMs of the binary nanohole array.

nanoholes can be regarded as electric dipoles collectively oscillating with the incident light. The coupling effects between neighboring nanoholes are relatively weak for the field mainly concentrating inside each nanohole. When the incident wavelength is 660 nm (Fig. 2(a)), the ALCR mode is excited, and the nanoholes in the two arrays oscillate with a phase difference of π. Because of the same strength of the resonant amplitude, the reradiated fields of two arrays strongly cancel each other out in the far field, and the coupling between the structure and free space light is largely minimized resulting in a Fano dip in transmission. At 740 nm (Fig. 2(b)), the ILCR mode dominates the radiation with nanoholes in two arrays oscillating in the same phase; thus, their reradiated fields interfere constructively and strongly couple with the incident light.

The Fano profiles are closely related to the radius difference of the binary nanohole array. Figs. 2(c) and 2(d) show the evolution of transmission spectra as R_1 increasing from 40 nm to 110 nm, while R_2 is fixed at 110 nm. As R_1 gets closer with R_2, the Fano profile gradually diminishes, while the resonance becomes much sharper with decreased linewidth and spectral contrast. Particularly, for the case of $R_1 = R_2$, the ALCR mode cannot be directly excited by normal incident light, and the Fano resonance disappears. To more clearly observe the evolution of the resonance, the spectral contrast defined as $(I_{peak} - I_{dip})/(I_{peak} + I_{dip})$ and the Q factor is employed to measure the lineshape. The Q factor defined by $Q = \omega_a/2W_a$ can be calculated by fitting the transmission spectra to the analytical model[33]

$$T = \frac{\left(\frac{\omega^2 - \omega_a^2}{2W_a\omega_a} + q\right)^2 + b}{\left(\frac{\omega^2 - \omega_a^2}{2W_a\omega_a} + q\right)^2 + 1} \times \frac{a^2}{\left(\frac{\omega^2 - \omega_s^2}{2W_s\omega_s} + q\right)^2 + 1}, \quad (1)$$

where ω is the angular frequency of the incident field, ω_a and ω_s are the resonant frequencies of Fano resonance and superimposed Lorentz resonance, respectively. W_a and W_s are the approximations of the spectral widths of both resonances in frequency units. q and a are the asymmetry parameter and maximum amplitude of the resonance, respectively. b is the modulation damping parameter originating from intrinsic losses.[33]

Fig. 3 shows the evolution of Q factor and spectral contrast as R_1 gets closer with R_2, and the Q factor and spectral contrast follow different evolution tendencies. As R_1 increases, the Q factor gradually increases (dark line in Fig. 3), indicating the increasing energy density of the electric field stored in the resonances of the system. However, the spectral contrast (red line in Fig. 3) reaches its highest value at small R_1 and decreases as R_1 gets larger. This is due to the fact that, in the binary nanohole array with small radius difference, the energy density of the electric field is much stronger, and a small loss introduced by silicon and ITO can result in a large dissipation of energy, which weakens the Fano profile and reduces the spectral contrast. In other words, lower R_1 means lower energy density of the electric field stored in the resonance of the binary nanohole array as well as lower dissipation and higher spectral contrast. The Q factors and spectral contrasts from

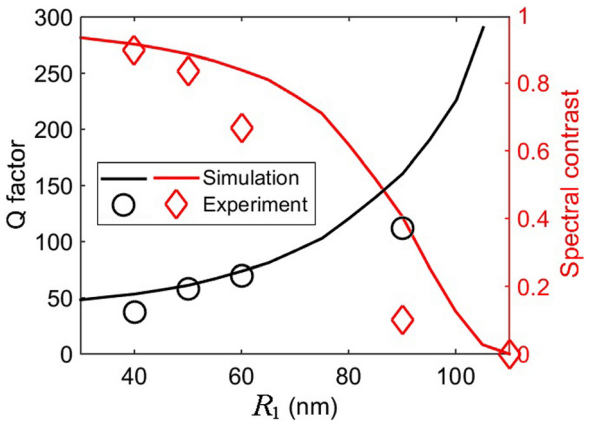

FIG. 3. Spectral contrast and Q factor evolution as R_1 gets closer with R_2.

experimental results agree well with the calculations, and the slight deviation is mainly due to the broadening of linewidth of the resonances and stray light caused by fabrication defects and imperfections. The ability of such structure to achieve high Q factor while still maintaining relatively high spectral contrast is especially beneficial to improve the performance of the Fano resonance based devices.

In order to realize Fano resonance based optical modulator, commercial nematic LC, E7, is chosen as the active media due to its large birefringence (~0.2) and various driven methods such as electrical field, acoustic wave, heat, and light. For simplicity, here, we adopt the electric field to drive the LC molecule realignment. The underlying tuning mechanism is shown in Fig. 4(a), the binary nanohole array and ITO glass form a LC cell. The LC molecules exhibit uniaxial optical symmetry with two principal refractive indices n_o and n_e. The ordinary refractive index n_o is for the light with electric field polarization perpendicular to the director and the extraordinary refractive index n_e is for the light with electric field polarization parallel to the director. When no voltage is applied, the rod-like LC molecules reside randomly between the two ITO layers and form a domain structure, where LC molecules preferably align in the same direction within one domain and vary randomly from domain to domain. Macroscopically (in the scale much larger than the domain size), the LC molecules can be characterized as an effective media with average refractive index of n_a. However, when a bias voltage is applied between the ITO layer, electric dipoles are formed by one end of a molecule having a net positive charge, while the other end has a net negative charge. As a result, the dipole molecules tend to orient themselves along the direction of the field. Consequently, the surrounding dielectric environment seen by the binary nanohole array is actively controlled by the applied voltage. The change in dielectric environment usually causes a shift in resonance wavelength, thus, for a certain wavelength, huge variation of transmission under different applied voltages can be envisioned. In the simulations, the rod-like LC molecules are modeled as an effective material with refractive index of n calculated with the help of the macroscopic order parameter q[1]

$$n = n_a - \frac{1}{3}\Delta n q, \quad (2)$$

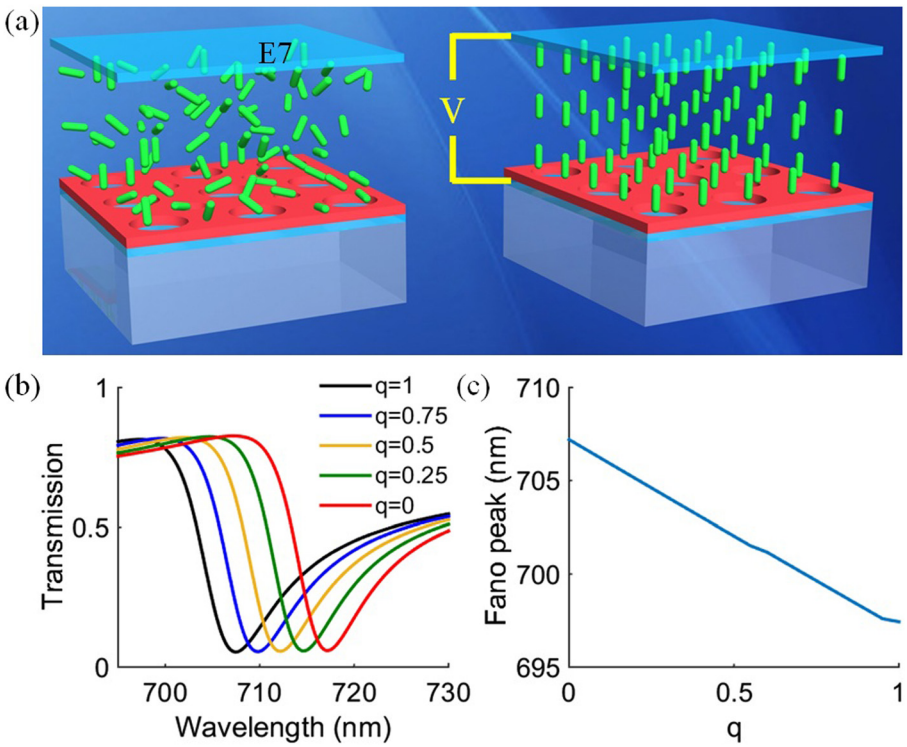

FIG. 4. (a) Schematics of active control of the Fano resonance based optical modulator. E7 LC molecules rearrange from random state to uniform state under an applied voltage. (b) Transmission and (c) Fano peaks for different macroscopic order parameter q ($R_1 = 50\,\text{nm}$ and $R_2 = 110\,\text{nm}$).

where $n_a = (2n_o + n_e)/3$ is the average refractive index of the unaligned LC and $\Delta n = n_e - n_o$ is the LC birefringence ($n_e = 1.734$ and $n_o = 1.525$ for E7). By applying voltage, the macroscopic order parameter changes from 0 (unaligned sample) up to 1 (fully aligned state) and the effective refractive index varies from n_a to n_o, respectively.

Fig. 4(b) shows the simulated transmission spectra for LC molecules under different macroscopic order parameter q ($R_1 = 50\,\text{nm}$ and $R_2 = 110\,\text{nm}$). One can notice that the incorporation of LC results in a sharp Fano profile with narrower width, higher spectral contrast, and resonance wavelength having a red shift due to the refractive index matching of the dielectric media on both sides. As the LC molecules tend to realign along the direction of the applied electrical field, the effective refractive index seen by the binary nanohole array gradually decreases, resulting in a blue shift of the profile. This is because the light field in the binary nanohole array is dominated by its X and Y components, as the orientation direction of the LC molecules rearrange from random state to uniform state along the applied electric field; the effective refractive index experiences a variation from n_a to n_o. Fig. 4(c) shows the wavelength of the Fano peak for LC molecules under different macroscopic order parameter q. 10 nm shift of resonance wavelength can be achieved with q changing from 0 to 1, which is wider than the linewidth of the Fano resonance.

To experimentally verify the numerical results, the LC cell is prepared by forming the binary nanohole array with ITO glass using a 31 μm spacer, and the infiltration process is done under 80 °C in vacuum environment through capillary action. After infiltration, the sample is slowly cooled down to room temperature with air pressure recovered to normal in order to push the LC molecules into the nanoholes. Figs. 5(a) and 5(b) show the measured transmission spectra of the binary nanohole array under different applied voltages. The evolution of the spectra is in good agreement with our theoretical analysis. The transmission dip blueshifts gradually from 722.5 nm to 713 nm as the applied voltage increases, and 26.7 kV/cm voltage is enough to shift the resonance from Fano peak to Fano dip. The Q factor keeps almost unchanged with the variation of applied voltage (Fig. 5(c)). The maximum modulation depth of 85% is achieved at 713 nm as shown in Fig. 5(d). The transmission monotonously decreases with the increased voltage, and the most rapid change of transmission is for the applied voltage around 10 kV/cm. At higher voltage, the variation saturates

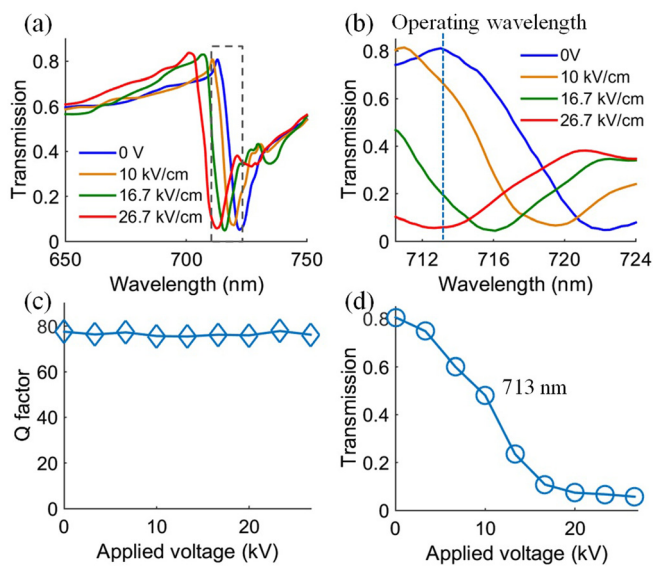

FIG. 5. (a) Transmission of the binary nanohole array and (b) its partial enlargement. (c) Q factors of the Fano resonance under different applied voltages. (d) Transmission at the operating wavelength (713 nm) under different applied voltages.

because the nematic LC molecules are almost completely aligned along the electric field.

In summary, the Fano resonance within a binary nanohole array composed of two nanohole arrays with different radii are studied both numerically and experimentally. Simulations using finite difference time domain method demonstrate that the origin of such sharp resonance is from the interaction of the hybridized ALCR mode and ILCR mode. Measured transmission spectra agree very well with the simulation results and show a different evolution tendency of Q factor and spectral contrast against the radius difference of the two nanohole arrays. Taking advantage of the easy tuning mechanism of E7 and the high Q factor and spectral contrast of the resonance, such binary nanohole array can act as a high performance optical modulator. The transmission of the operating wavelength monotonously decreases with the increasing applied voltage; an unprecedented modulation depth of 85% is achieved.

This work was supported by the National Natural Science Foundation of China under Grant Nos. 50836002 and 51176041. The authors would like to thank the assistance from the Laboratory of Microfabrication, Institute of Physics, Chinese Academy of Sciences on the sample fabrication.

[1]G. Y. Si, Y. H. Zhao, E. S. Leong, and Y. J. Liu, Materials **7**(2), 1296 (2014).
[2]Y. H. Sun, L. Jiang, L. B. Zhong, Y. Y. Jiang, and X. D. Chen, Nano Res. **8**(2), 406 (2015).
[3]O. Hess, J. B. Pendry, S. A. Maier, R. F. Oulton, J. M. Hamm, and K. L. Tsakmakidis, Nat. Mater. **11**(7), 573 (2012).
[4]A. D. Boardman, V. V. Grimalsky, Y. S. Kivshar, S. V. Koshevaya, M. Lapine, N. M. Litchinitser, V. N. Malnev, M. Noginov, Y. G. Rapoport, and V. M. Shalaev, Laser Photonics Rev. **5**(2), 287 (2011).
[5]H. Jing, Q. F. Zhang, N. Large, C. M. Yu, D. A. Blom, P. Nordlander, and H. Wang, Nano Lett. **14**(6), 3674 (2014).
[6]N. Strohfeldt, A. Tittl, M. Schaferling, F. Neubrech, U. Kreibig, R. Griessen, and H. Giessen, Nano Lett. **14**(3), 1140 (2014).
[7]H. A. Atwater and A. Polman, Nat. Mater. **9**(3), 205 (2010).
[8]L. Li, U. Steiner, and S. Mahajan, Nano Lett. **14**(2), 495 (2014).
[9]A. Baba, K. Tada, R. Janmanee, S. Sriwichai, K. Shinbo, K. Kato, F. Kaneko, and S. Phanichphant, Adv. Funct. Mater. **22**(20), 4383 (2012).
[10]G. A. Wurtz, P. R. Evans, W. Hendren, R. Atkinson, W. Dickson, R. J. Pollard, A. V. Zayats, W. Harrison, and C. Bower, Nano Lett. **7**(5), 1297 (2007).
[11]Z. L. Samson, K. F. MacDonald, F. D. Angelis, B. Gholipour, K. Knight, C. C. Huang, E. D. Fabrizio, D. W. Hewak, and N. I. Zheludev, Appl. Phys. Lett. **96**(14), 143105 (2010).
[12]Y. J. Liu, G. Y. Si, E. S. Leong, N. Xiang, A. J. Danner, and J. H. Teng, Adv. Mater. **24**(23), OP131 (2012).
[13]L. Z. Yang, C. Y. Pei, A. Shen, C. Y. Zhao, Y. Li, T. G. Dai, H. Yu, Y. B. Li, X. Q. Jiang, and J. Y. Yang, Appl. Phys. Lett. **104**(21), 211104 (2014).
[14]F. Zhang, X. Y. Hu, C. Y. Wu, H. Yang, and Q. H. Gong, Appl. Phys. Lett. **105**(18), 181114 (2014).
[15]P. R. Evans, G. A. Wurtz, W. R. Hendren, R. Atkinson, W. Dickson, A. V. Zayats, and R. J. Pollard, Appl. Phys. Lett. **91**(4), 043101 (2007).
[16]A. Minovich, J. Farnell, D. N. Neshev, I. McKerracher, F. Karouta, J. Tian, and Y. S. Kivshar, Appl. Phys. Lett. **100**(12), 121113 (2012).
[17]O. Buchnev, N. Podoliak, M. Kaczmarek, N. I. Zheludev, and V. A. Fedotov, Adv. Opt. Mater. **3**(5), 674 (2015).
[18]O. Buchnev, J. Y. Ou, M. Kaczmarek, N. I. Zheludev, and V. A. Fedotov, Opt. Express **21**(2), 1633 (2013).
[19]M. Decker, C. Kremers, A. Minovich, I. Staude, A. E. Miroshnichenko, D. Chigrin, and Y. S. Kivshar, Opt. Express **21**(7), 8879 (2013).
[20]B. Luk'yanchuk, N. I. Zheludev, S. A. Maier, N. J. Halas, P. Nordlander, H. Giessen, and C. T. Chong, Nat. Mater. **9**(9), 707 (2010).
[21]A. E. Miroshnichenko, S. Flach, and Y. S. Kivshar, Rev. Mod. Phys. **82**(3), 2257 (2010).
[22]B. B. Zeng, Y. K. Gao, and F. J. Bartoli, Appl. Phys. Lett. **105**(16), 161106 (2014).
[23]W. Y. Zhao, X. D. Leng, and Y. Y. Jiang, Opt. Express **23**(5), 6858 (2015).
[24]J. Ye, F. F. Wen, H. Sobhani, J. B. Lassiter, P. V. Dorpe, P. Nordlander, and N. J. Halas, Nano Lett. **12**(3), 1660 (2012).
[25]Y. Y. Huo, T. Q. Jia, Y. Zhang, H. Zhao, S. A. Zhang, D. H. Feng, and Z. R. Sun, Appl. Phys. Lett. **104**(11), 113104 (2014).
[26]W. Y. Zhao, D. Q. Ju, Y. Y. Jiang, and Q. W. Zhan, Opt. Express **22**(25), 31277 (2014).
[27]B. Slovick, Z. G. Yu, M. Berding, and S. Krishnamurthy, Phys. Rev. B **88**(16), 165116 (2013).
[28]J. Cheng, D. Ansari-Oghol-Beig, and H. Mosallaei, Opt. Lett. **39**(21), 6285 (2014).
[29]A. García-Etxarri, R. Gómez-Medina, L. S. Froufe-Pérez, C. López, L. Chantada, F. Scheffold, J. Aizpurua, M. Nieto-Vesperinas, and J. J. Sáenz, Opt. Express **19**(6), 4815 (2011).
[30]E. D. Palik, *Handbook of Optical Constants of Solids* (Academic Press, 1998).
[31]R. A. Synowicki, Thin Solid Films **313–314**, 394 (1998).
[32]A. B. Evlyukhin, C. Reinhardt, A. Seidel, B. S. Luk'yanchuk, and B. N. Chichkov, Phys. Rev. B **82**(4), 045404 (2010).
[33]B. Gallinet and O. J. Martin, ACS Nano **5**(11), 8999 (2011).